Self-healing and Crack-sealing Ability of 30-Day-Long 300°C Cured Thermal Shock Resistant Cement Composites

Tatiana Pyatina and Toshifumi Sugama

Brookhaven National Laboratory

Keywords: *self-healing, re-adhering, corrosion protection, calcium aluminate cement, fly ash F.*

ABSTRACT

This paper is the last in the series of works on self-healing cement composites for high-temperature geothermal well applications presented by Brookhaven National Laboratory. It focuses on long-term self-healing properties of earlier developed Thermal Shock Resistant Cement (TSRC) composite non-modified and modified with Micro Glass Fibers (MGF). Previous studies demonstrated some outstanding self-healing properties of this composite after short initial curing of 1 day, repeated compressive damage and 5-day recovery periods at 300°C. In this work, we studied ability to recover strength, Youngs Modulus (YM) and seal cracks after compressive damage imposed on MGF-modified and non-modified TSRC composites after initial autoclaving time of up to 30 days at 300°C. The TSRC performance was compared against that of OPC/SiO_2 composite. Non-modified 30-day 300°C-cured TSRC composite demonstrated 86% recovery of compressive strength after the damage. MGF-modified 30-day aged TSRC had a considerably (nearly 3-fold) increased YM and compressive strength increased by 1.6 times compared with that of 1-day-aged composite, leading to the alterations in mechanical behavior from moderate brittleness to true brittle nature resulting brittle failure under the stress. Correspondingly, the recovery of compressive strength was only 61% compared with 86% recovery of unmodified TSRC at the same curing age. However, MGF-modified TSRC 30-day cured and then damaged TSRC showed a better sealing ability than TSRC damaged after 1 day of curing. This fact strongly suggested that the disintegration of MGF in TSRC composite is very slow even at 300°C, thereby ensuring the sealing feasibility at later times. Thus, the lack of strength recovery may be due to the larger cracks and formation of these new iron-related reaction products, but independent of excellent crack sealing efficacy.

1. Introduction

In hostile geothermal environments containing hypersaline brine, CO_2 and H_2S at temperatures >250°C, the well cement sheath between the casing and rock/clay formation frequently encounters variable mechanical-and chemical stresses leading to micro-annuli and cracks, increased cement permeability, cement debonding from the casing and formation, casing corrosion by geothermal fluids migrating through cement and compromised zonal isolation (Amin, Kim, Lee, & Kim, 2009; Teodoriu, Kosinowski, Amani, Schubert, & Shadravan, 2013;

Zhijun, Yanjun, & Jianghong, 2013). Repairs of well cements are complicated, costly and sometimes impossible since the cement failure locations are challenging to find, to reach and to repair correctly.

Cement technologies able to self-heal cracked cement matrix may deal with these issues. Currently, there are several technical strategies for developing self-healing cements in the building and construction industries, as well as oil and gas fields, at temperatures ranging from 20^{o} to 140^{o}C. Among them, the autogenous- and autonomic- or combined-healing technologies may be applicable to geothermal well cements facing the high-temperature hydrothermal environments. The former strategy relies on hydration of residual non-hydrated and partially hydrated cement particles by permeation of water through micro-annuli or cracks, and the carbonation of hydrated products. The hydration and carbonation reaction products grow as amorphous and crystalline phases, sealing the openings (Edvardsen, 1999; Huang, Ye, & Damidot, 2013). In autonomic healing, materials are added specifically for the purposes of self-healing, such as pozzolanic cementitious materials (Huang, Ye, & Damidot, 2014; M. G. Sahmaran, Yildirim, & Erdem, 2013) and expansive additives (Ahn & Kishi, 2010; Sisomphon, Copuroglu, & Koenders, 2012). In contact with water penetrating through defects, these healing aids dissolve, hydrate and precipitate new products sealing the cracks. The size of the cracks is an important parameter of cement's self-healing behavior. The cracks that heal in short periods of time under ambient conditions are typically below 60 μm in width (Li & Yang, 2007; Reinhardt & Jooss, 2003). Thus, the control of crack widths is one of the key factors for a successful self-healing process. To control cracks formation and propagation, various fibers are commonly added to cement formulations (Sui et al., 2018; Y. Yang, Michael, Yang, & Li, 2009). Micro-carbon fibers (MCF), moderately reacting with the cement matrix of alkali-activated calcium aluminate cement (CAC)/Class F fly ash (FAF) blend, effectively increased cement toughness of the blend at 270°C and provided excellent bridging control of crack development, propagation, and post-stress cracks' opening (Pyatina & Sugama, 2014b, 2015).

This blended cement system was developed as thermal shock-resistance cement (TSRC) for both conventional geothermal reservoirs and Enhanced Geothermal System (EGS) wells with large temperature variations (Gill, Pyatina, & Sugama, 2012; Pyatina & Sugama, 2014a). FAF in this system initially acted as a temporary filler improving packing and densifying the matrix formed with the first binding phases of CAC hydrates at an early curing stage. After longer curing, the dissolution of FAF by the alkaline activator, sodium metasilicate, followed by the pozzolanic reactions, led to the formations of amorphous sodium-, calcium-, or sodium/calcium-aluminosilicate, Na_2O-, CaO- or Na_2O/CaO-Al_2O_3-SiO_2-H_2O, [(N, C, or N/C)-A-S-H)] gels as secondary binding phases. Furthermore, even when the cement was autoclaved at high hydrothermal temperature of 300°C, the pozzolanic reactions of FAF were relatively slow. In fact, substantial amounts of non-reacted and partially reacted spherical FAF particles remained in cement matrix after a 10-day-autoclaving. This could aid self-healing even in aged cement.

MCF-reinforced TSRC showed outstanding compressive strength recoveries of more than 84% for cement samples compressively damaged after 1-day curing at 270^{o}C in water or sodium carbonate and exposed to the same conditions for 5 more days after the damage (Pyatina, Sugama, & Ronne, 2016). Recoveries of compressive strength of OPC high-temperature composites under the same conditions ranged between 54 and 67%. Sealing of 0.25 mm wide

cracks was also far greater for the TSRC than for OPC as seen by three-dimensional micro-image analyses.

In this paper, the ability of TSRC and TSRC modified with MGF to self-heal after longer initial curing time of 30 days at 300^{o}C is investigated. Performance of these two composites in Young's modulus and compressive strength recovery is compared against that of OPC/SiO_2 common high-temperature well cement blend. The major concern for long-term cured composites is diminished capacity of slow-reacting additives especially at high temperatures. Additionally, the nature of the composites themselves changes with time because of the increased strength and decreased flexibility. These changes may significantly diminish self-healing ability of TSRC composite that showed outstanding recoveries after short curing times.

2. Experimental procedure

2.1. Materials

Calcium-aluminate cement (CAC) #80 and Class F fly ash (fly ash F, FAF) were supplied by Kerneos Inc. and Boral Material Technologies, Inc. SMS (Na_2SiO_3), alkali-activating powder, of 93% purity, with the particles' size of 0.23- to 0.85-mm, trade named "MetsoBeads 2048," was supplied by the PQ Corporation. It had a 50.5/46.6 Na_2O/SiO_2 weight ratio. Schlumberger Inc. provided Dyckerhoff, class G cement and silica flour. Micro carbon-fibers (MCF, AGM-94) derived from a polyacrylonitrile precursor, were supplied by Asbury Graphite Mills, Inc. The size of individual fiber was 7-9 μm in diameter and 100-200 μm in length. E-type MGF (Microglass 7280) with fiber diameter of 16 μm and length of 120 μm was supplied by Fibertec. The oxide composition of this MGF as aluminum-lime silica system determined by energy-dispersive X-ray (EDX) analysis was as follows: 55.0wt% SiO_2, 28.6wt% CaO, 11.4wt% Al_2O_3, 2.8wt% MgO, 0.9wt% Fe_2O_3, 0.7wt% TiO_2, and 0.6wt% Na_2O.

The dry blend of TSRC consisted of 34.5% FAF, 51.5% CAC#80, 5.5% SMS and 8.5% MCF. For the blend with MGF half of the MCF was replaced by MGF. Both blends were hand-mixed with water at water-to-blend ratio of 0.45.

The compressive strength and Young's modulus were determined on samples prepared in the following sequence: the hand-mixed slurries were poured in cylindrical molds (20 mm diam. and 40 mm height), and left to harden for 24hrs at room temperature; the hardened cements were removed from the molds, and placed in a 100% relative humidity (R.H.) environment at 85°C for 24hrs; finally, the samples were autoclaved for 30 days at 300°C under pressure of 8.3 MPa. (The longest curing time possible within the framework of the project at the highest available temperature and pressure were selected.)

2.2. Measurements

The self-healing performance for the 300°C-atuclaved cylindrical samples was evaluated in the following manners. Firstly, mechanical tests to measure compressive strength and Young's modulus and damage the samples were conducted by Electromechanical Instron System Model 5967. In these tests, the machine was stopped within no more than 40% of compressive strain after the yield point. Such operation essentially avoided severe damage that would produce crumbled samples (Pyatina et al., 2016). Next, the cracked samples were autoclaved for 5 additional days at 300^{o}C, and thereafter, compressive strength and Young's modulus of these

samples were measured. Each test result was the average of at least three samples. These tests provided the recovery rate of strength as one of the factors needed for evaluation of the self-healing performance. For XRD, the samples were examined using a 40 kV, 40 mA copper anode X-ray tube. The results were analyzed using PDF-4/Minerals 2015 database of International Center for Diffraction Data (ICDD). Nikon Eclipse LV 150 3-D microscope was employed to obtain visual images of crack's sealing and to explore the microstructures developed in sealed cracks. The identification of the crystalline products accumulated in the cracks during the 5-day healing was made by Raman chemical state mapping experiments concomitant with a Renishaw® in Via™ confocal Raman microspectrometer equipped with Leica® DM2700™ upright microscope.

3. Results and interpretations

3.1. Strength recovery

We evaluated YM and compressive strength of MGF-modified and non-modified TSRC composites after longer autoclaving time of up to 30 days at 300°C and their recovery after compressive damage and additional 5 days of healing under these conditions. For comparison, OPC/SiO_2 composite, was employed in this work. YM of OPC/SiO_2 increased in the first 15 days to 268 x 10^3 psi, and somewhat declined to 249 x 10^3 psi after 30 days (Figure 1). Nevertheless, after 30 days autoclaving, this composite was moderately brittle in nature. The YM of TSRS free of MGF increased with an extended autoclaving time from 126 x 10^3 psi after 1-day to 204 x 10^3 psi after 30 days in an autoclave. In contrast, a conspicuous increase of YM was observed for MGF-modified TSRC composite after longer autoclaving; YM value increased by nearly 3-fold to 409 x 10^3 psi after a 30-day autoclaving, compared against the 1-day autoclaved composite, thereby resulting in mechanical transition from moderate brittle nature to brittle one due to alkali dissolution and reactions of MGF, followed by densification of cement.

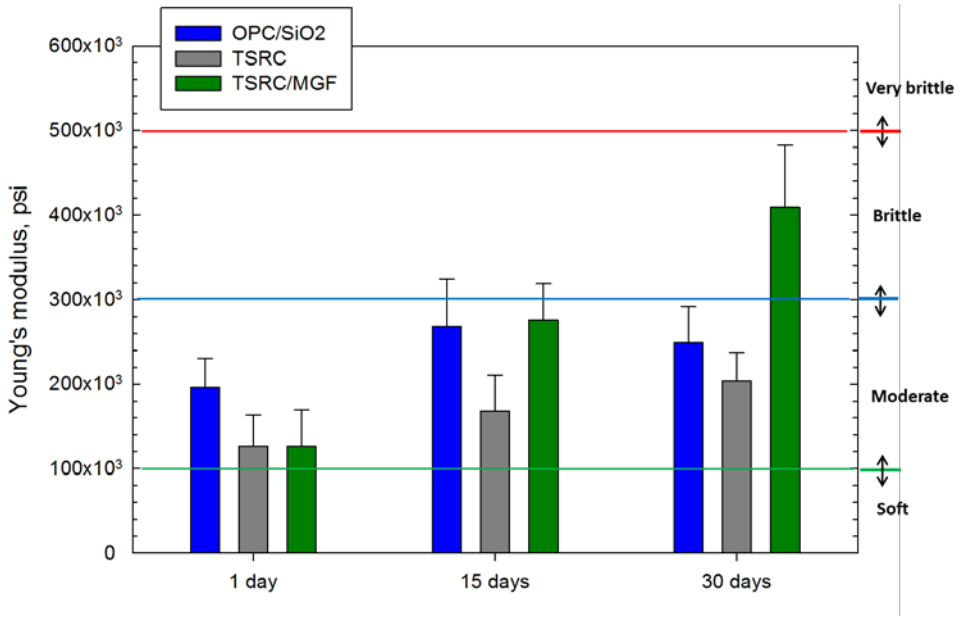

Figure 1: YM of 1-, 15-, and 30-day-autoclaved MGF-modified TSRC, unmodified TSRC and OPC/SiO_2 reference composite.

Figure 2 gives the compressive strength of 1-, 15-, and 30-day-autoclaved composites before and after a 5-day self-healing treatment. The compressive strength measurements results were similar to YM data; namely, two composites, TSRC and MGF-modified TSRC, exhibited increase in compressive strength as a function of autoclaving time. The strength increased to 2410 psi after 30 days from 1740 psi after 1 day for TSRC and to 2860 psi after 30 days from 1840 psi after 1 day for the TSRC/MGF one. On the other hand, for OPC/SiO_2 reference, the highest strength of 3320 psi was developed after 15 days; however, extending the autoclaving period to 30 days engendered some reduction of the strength to 2965 psi.

Figure 3 represents the compressive strength recovery after 300°C-5-day-self-healing treatment in plain water. The highest recovery of 117% was observed for 1-day-autoclaved TSRC/MGF composite, strongly suggesting that MGF acts as a very effective healing aid at early autoclaving age. However, the extended autoclaving time to 15 days resulted in the reduction of recovery rate to 84%, and a further reduction to 61% was observed for the 30-day-autoclaved sample. TSRC free of MGF showed no significant changes in strength recovery, which ranged from 81 to 86%, for 1-, 15-, and 30-day autoclaved composites. Meanwhile, the average recovery of 15- and 30-day-autoclaved OPC/SiO_2 reference was only 37%, which was 36% lower than that of 1-day autoclaved one. Thus, it appeared that the recovery of OPC/SiO_2 reference decreases after longer curing times.

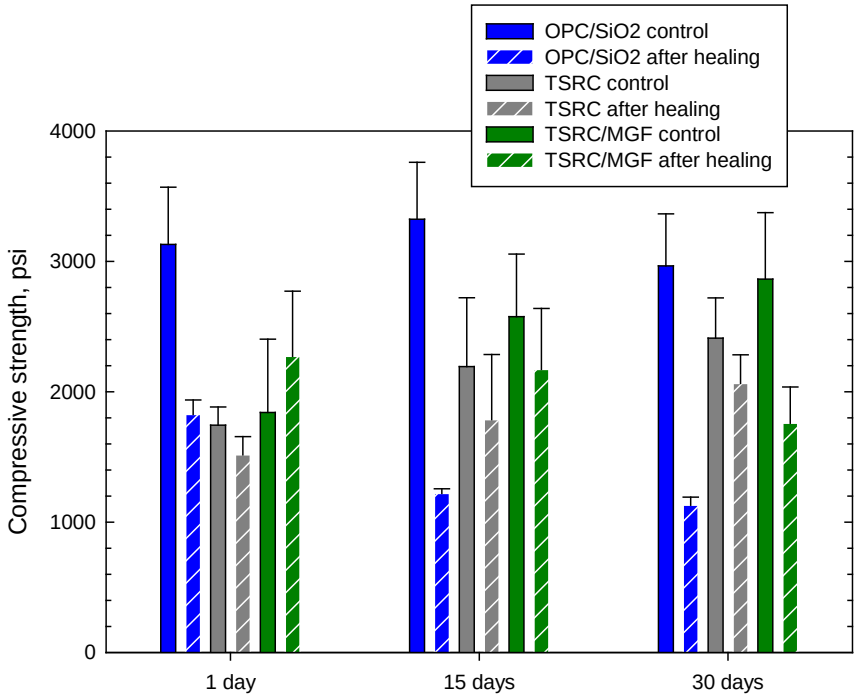

Figure 2. Compressive strength of MGF-modified TSRC, and unmodified TSRC and OPC/SiO_2 reference composite before and after 300°C-5-day-self-healing treatment.

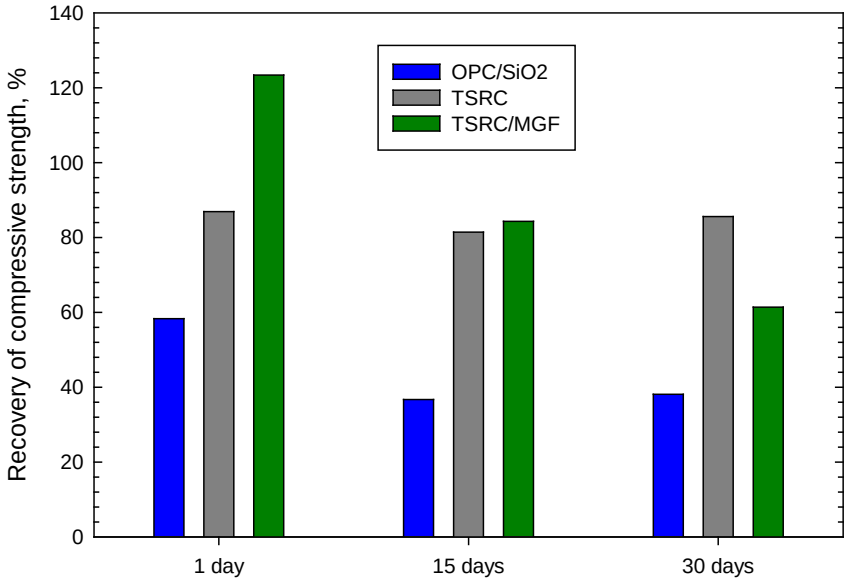

Figure 3. Recovery of compressive strength for MGF-modified TSRC, unmodified TSRC and OPC/SiO_2 reference composite after 300°C-5-day-self-healing treatment for composites with the first compressive damage imposed after 1-, 15- or 30 days of the initial curing at 300°C.

3.2 MGF-free TSRC after 15- or 30-day initial curing time: 3D micro-image analyses of cracks sealing

Figure 4 shows images of typical natural cracks with width, ranging from 0.1 to 0.2 mm, for TSRC composite samples without MGF cured in plain water at 300°C for 15 or 30 days before and after 5-day healing treatment. The 3D images show the crack's profiles with the depth in mm before and after the sealing (red numbers). In many cases the cracks were completely sealed, so they are not visible; moreover, the new particles were deposited on top of the original cracks forming protruding upwards structures (e.g. see the 3D image of 30-day TSRC-CF sample after 5-day healing in Figure 4). The blue arrow on the image of 5-day healed TSRC sample damaged after 15 days of curing marks the location of the original crack after the healing.

Moderately-sized cracks formed in TSRC and effectively sealed after only 5-day exposure to the original curing conditions when the damage was imposed after 15- and even 30 days of the initial curing (Note, a 10-day treatment was required to seal a slightly wider crack >0.2 mm in a 1-day cured sample, Figure 5.) The 30-day cured sample displayed increased surface roughness due to the deposition of new products after the additional 5 days of healing, and the small crack was effectively sealed.

The healing in terms of cracks sealing seemed to proceed faster for the samples with the longer initial curing before the imposed damage. It is reasonable to rationalize that FAF reacted further after 15 and 30 days compared with that of the 1-day cured samples. In this case, the reactive ions released by the thermo-alkaline activation of FAF would be more readily available to form new phases after longer curing times.

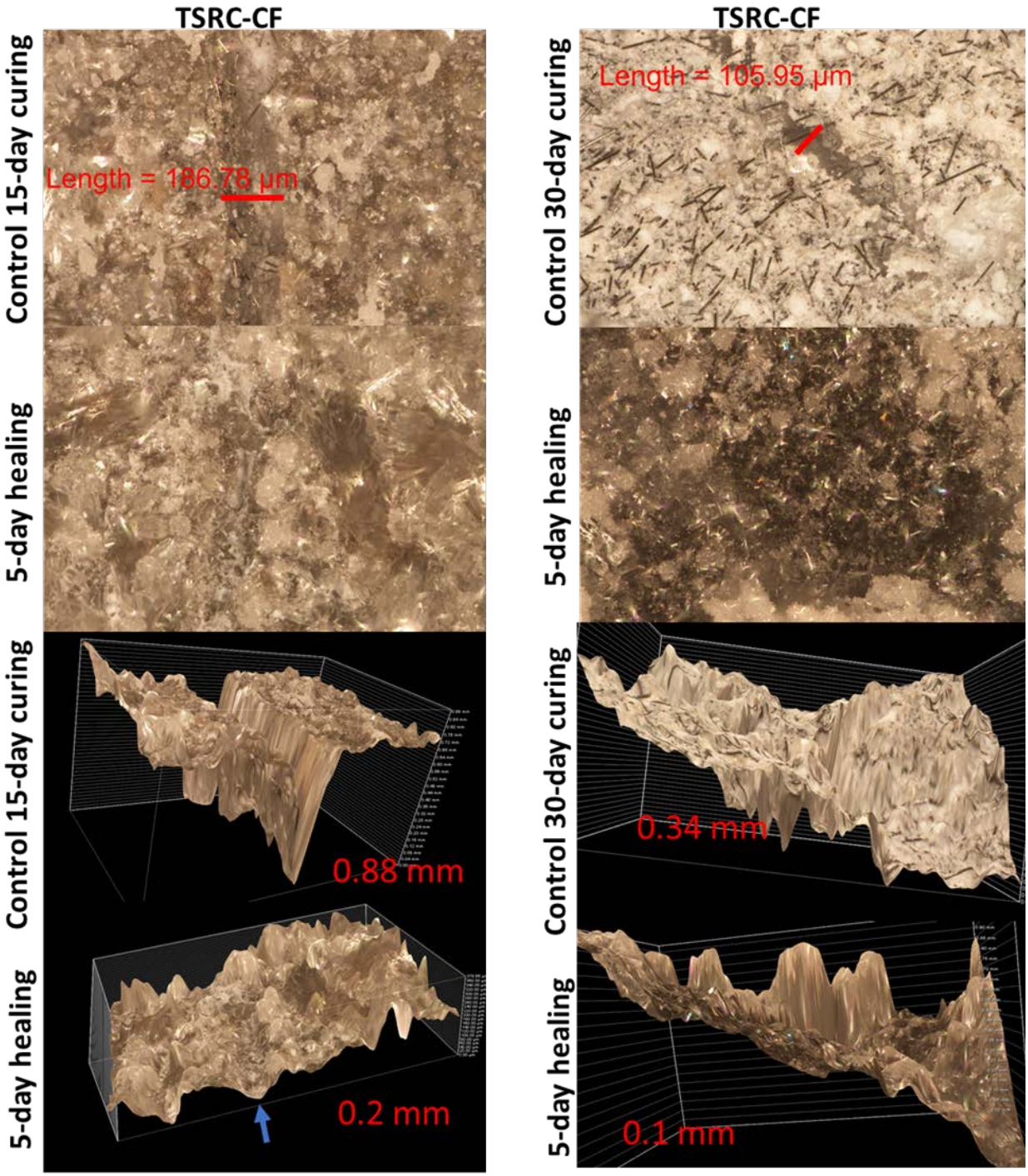

Figure 4. 15- and 30-day 300°C cured samples damaged and healed for another 5 days under the same conditions for TSRC.

On the other hand, the calcium-aluminate cement reaction products should be completely formed by that time and are unlikely to contribute significantly to the sealing of the cracks. Furthermore, when the initial FAF source would be exhausted at longer curing time, the phase transitions and reactions of FAF-derived reaction products with the environmental ions could further contribute to the cracks sealing.

3.3 MGF-modified TSRC after 1-, 15- or 30-day initial curing time: 3D micro-image analyses of cracks sealing

The incorporation of MGF into TSRC composite led to a highly increased YM and compressive strength with extended initial curing time compared against TSRC without MGF; particularly, YM value was in the region of brittle nature, ranging from 300 to 500 x 10^3 psi after 30 days initial curing, while 1- and 15-day cured samples had the moderate brittle nature.

Figure 5 compares the microstructures of typical cracks before and after their short-term sealing for MGF-modified TSRC (denoted as TSR-CF-GF) and unmodified one (TSRC-CF) samples cured for 1 day in 300^{o}C plain water and then healed for 5 or 10 days under the same environment after the imposed damage. As can be seen, the initial crack for modified sample was larger than that of unmodified one; for instance, a typical crack shown was 0.4 mm wide and 1.25 mm deep for the composite with MGF, and 0.25 mm wide and 0.7 mm deep for that without MGF. The smaller crack of the sample without MGF sealed completely in 10 days. That of MGF-modified sample was partially sealed after the 10-day treatment, its depth decreased by only ~30% at its deepest points. However, interestingly, the top shallow area of the crack was capped and bridged by reaction and precipitation products, so that a further sealing activity was no longer needed. Conceivably, these reaction and precipitation products may come from the thermo-alkali dissolution of MGF during the healing.

The sealing became more efficient for the MGF-modified samples after longer initial curing. As is evident from Figures 6 and 7, both cracks formed after 15 and 30-day initial curing for modified samples were wider than for unmodified samples. The formation of these wider cracks seems to represent a brittle fracture mode. Interestingly, both cracks were sealed after the 5-day treatment, instead of the 10-day treatment required for the damaged 1-day aged samples. The most likely explanation for this reduced healing time is a ready availability of reactive ionic species released by the slow continuous disintegration of MGF under alkaline environment of the composite at 300°C after long-term curing. These ionic reactants formed new sealing and plugging solid state phases in cracks possibly because of the interactions with the composite components.

Additionally, the increase in MGF's disintegration after longer curing time is likely to form amorphous phases which could help in filling the cracks. The excellent sealing performance of MGF-modified TSRC does not correlate with the low strength recovery of the long-term cured samples. This fact suggests that sealing phases do not contributed significantly to the strength recovery or/and other factor affected the strength recoveries.

3.4 Phase analyses of MGF-modified and unmodified TSRC in plain water

The major and minor crystalline phases formed in non-modified TSRC composite under steam at 300^{o}C after 1-day (control) and long-term curing are given in Table 1 for matrix and Table 2 for the surface.

The crystalline phases after the first day of curing included grossular hydroxylian, zeolite, analcime, feldspar mineral dmisteinbergite, some boehmite, and non-reacted species of corundum and mullite. The patterns noticeably changed after longer curing times of 15 and 30 days. Carbonated-sodium-calcium-aluminum silicate (sodium-calcium cancrinite) replaced analcime, the peaks' intensities of dmisteinbergite, katoite and mullite decreased. (Note, that multiple grossular peaks indicated various stoichiometries of hydrogrossular.) Decomposition of mullite contributed to the formation of calcium-magnesium-iron-aluminum silicates (clintonite from mica group and possibly, khesinite – two small peaks of these mineral at 2Θ: 10.93 and 11.88 do not overlap with any other phases). After the 30-day curing, aluminum in grossular was partially substituted by ferric ion to form grossular ferrian hydroxylian.

Additionally, as is evident from increasingly intense signal at 2Θ: 35.72-36, the released iron crystallized as maghemite. Decomposition of FAF also resulted in increased boehmite peaks intensities and a new peak at 2Θ: 30.26 from SiO_2 (stishovite) as well as a small peak after 30 days attributed to quartz. A strong peak at 2Θ of 20.26, partially overlapping with the dmisteinbergite peak at 20.18 was likely from some mica-type mineral. The intensity of the peak stayed the same after the 15 and 30 days of curing. Because of the complex multi-phase composition, it was difficult to ascribe this peak to an exact phase. Similarly, the increased quartz signal after longer curing times complicated evaluation of the intensity of residual mullite peaks strongly overlapping with other phases and, in particular, with silica at ~2Θ of 26.

In summary, at longer exposure of unmodified TSRC to high-temperature hydrothermal conditions, FAF further reacted with the release of aluminum, silicon, iron and magnesium ions that participated in phase transitions and formation of new minerals. The minerals such as iron-containing grossular further reinforced the matrix providing cement strength recovery even after long initial curing times, while the dissolution and precipitation of silica acted to seal the cracks. Some minerals participated in both strength recoveries and cracks sealing (cancrinite and boehmite). The complexity of XRD patterns did not allow a definite conclusion on whether some crystalline FAF was left after the 30 days of curing. Some peaks could be ascribed to feldspars with decreased calcium (albite, calcian) or alkali feldspars (albite, orthoclase, sanidine).

The major crystalline surface phase was silica. High intensity of silica peaks complicated identification of other significantly smaller peaks. These were ascribed to sodium-iron-aluminum silicate or sodium-aluminum silicate, aegirine (a product of MGF alkaline decomposition); zeolites, analcime and amicite; aluminum-oxide-hydroxide, boehmite and mica-type mineral, paragonite with limited certainty. Likewise, some peaks could be from feldspars with decreased calcium (albite, calcian) or alkali feldspars (albite, orthoclase, sanidine). These minerals crystallized after most calcium from CAC already reacted and only FAF participated in the formation of new phases.

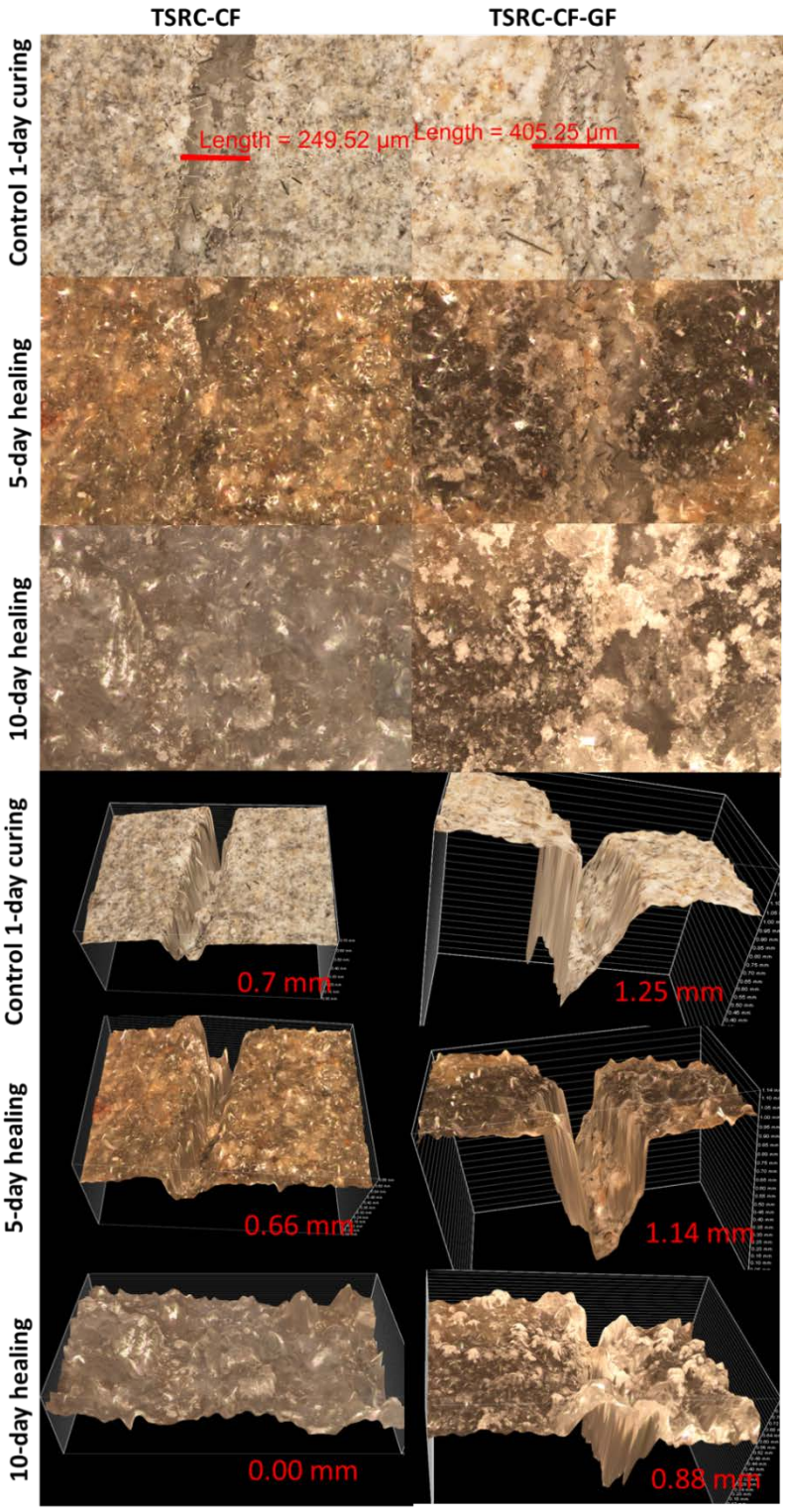

Figure 5. Comparison of short-term cracks sealing for TSRC samples modified with micro-carbon fibers (CF) (left) and both carbon and glass fibers (GF) (right) at 300°C in water. The cracks formed after 1-day 300°C hydrothermal curing of the samples.

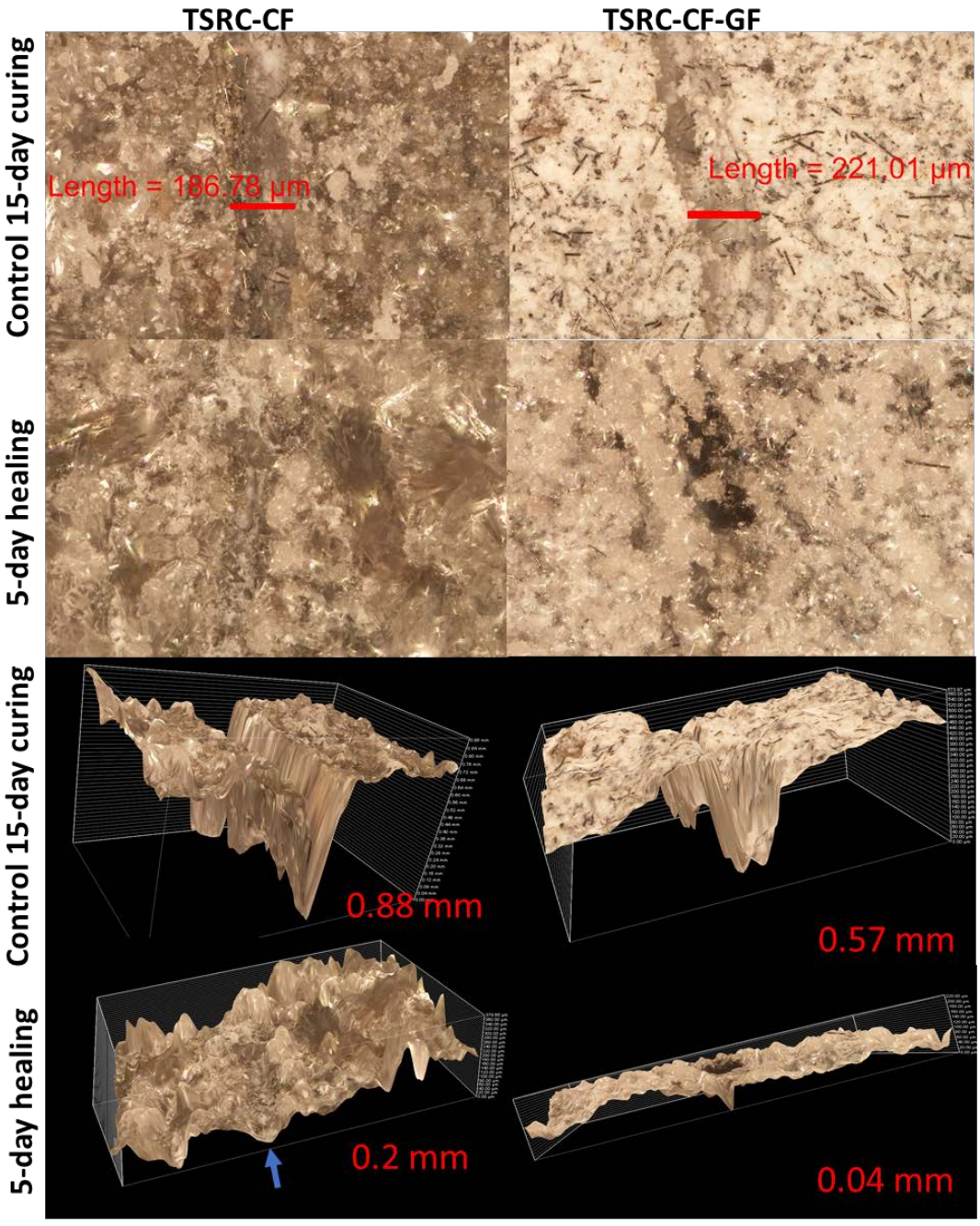

Figure 6. 15-day 300°C cured samples damaged and healed for another 5 days under the same conditions for unmodified TSRC and TSRC modified with MGF.

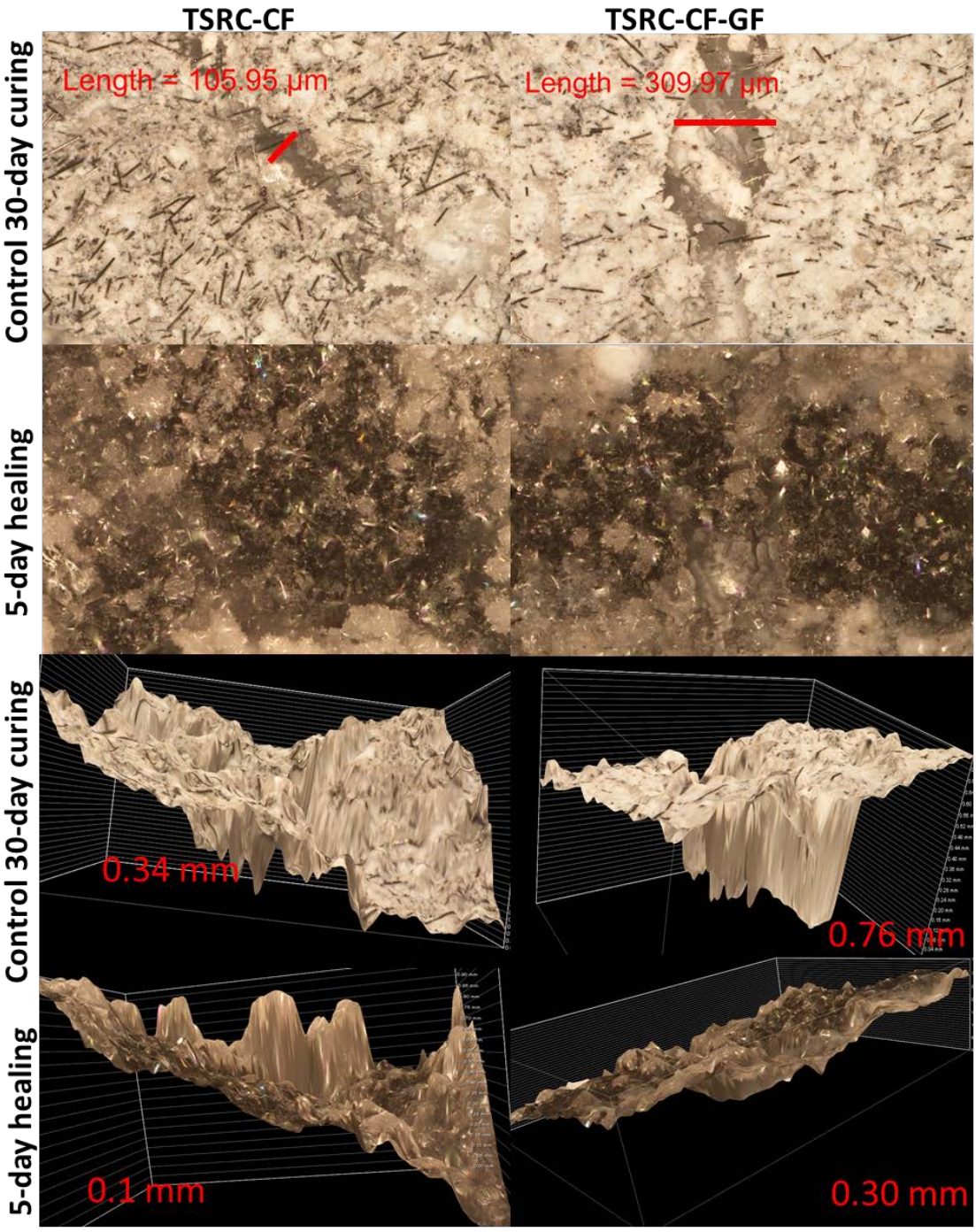

Figure 7. 30-day 300°C cured samples damaged and healed for another 5 days under the same conditions for unmodified TSRC and TSRC modified with MGF.

Table 1. Major, minor and possible crystalline phases formed in matrix at 300°C after 1-, 15- or 30-day exposure of unmodified TSRC.

Major phases (ICDD numbers)	Minor phases (ICDD numbers)
1-day curing	
Analcime, $Na_{0.9}((Al_{0.9}Si_2)O_6)(H_2O)$ (01-076-6569)	Boehmite AlOOH (04-012-5050)
Grossular hydroxylian $Ca_3Al_2(SiO_4)_2(OH)_4$ (and other stoichiometries) (00-042-0570)	Mullite $Al_{2.25}Si_{0.75}O_{4.875}$ (04-014-8459)
Katoites $Ca_{2.916}Al_2Si_{1.092}O_{12}H_{7.632}$/ $Ca_3Al_2(SiO_4)_{1.53}(OH)_{5.88}$ (01-075-4213/04-014-984)	
Dmisteinbergite $CaAl_2Si_2O_8$ (04-011-5220)	
Corundum Al_2O_3 (01-073-1512)	
15-day curing	
Cancrinite $Na_{7.28}Ca_{0.64}(Si_6Al_6O_{24})(CO_3)_{1.65}(H_2O)_2$ (01-081-9895)	Boehmite AlOOH (04-012-5050)
Grossular hydroxylian $Ca_3Al_2(SiO_4)_2(OH)_4$ (and other stoichiometries) (00-042-0570)	Andradite $Ca_3Fe_2(SiO_4)_3$ (04-012-1284)
Clintonite $CaMg_{2.3}Fe_{0.1}Al_{3.2}Si_{1.4}O_{10}(OH)_2$ (04-019-1584)	Mullite $Al(Al_{0.83}Si_{1.08}O_{4.85})$ (01-089-2645)
Some mica mineral	Corundum Al_2O_3 (04-015-8610)
	Stishovite SiO_2 (00-045-1374)
	Possible:
	Khesinite $CaMgFe_{2.2}Al_{1.7}Si_{1.1}O_{10}$ (04-013-3515)
30-day curing	
Grossular ferrian hydroxylian $Ca_3Al_{1.096}Fe_{0.904}(Si_{2.823}O_{11.292})(OH)_{0.708}$ (and other stoichiometries) (01-072-8446)	Sodium aluminum silicate hydrate $Na_8(AlSiO_4)_6(OH)_2$ (00-040-0100)
Cancrinite $Na_{7.28}Ca_{0.64}(Si_6Al_6O_{24})(CO_3)_{1.65}(H_2O)_2$ (01-081-9895)	*Possible*:
Bohmite AlOOH (04-014-2197)	Albite $Na(AlSi_3O_8)$ (04-007-5009)
Corundum Al_2O_3 (04-008-3293)	Anorthoclase $(Na,K)(Si_3Al)O_8$ (00-009-0478)
Silicon oxide/quartz SiO_2 (01-077-8624/04-007-1808)	Khesinite $CaMgFe_{2.2}Al_{1.7}Si_{1.1}O_{10}$ (04-013-3515)
Some mica mineral	Foshagite $Ca_4(SiO_3)_3(OH)_2$ (00-029-0377)
	Clintonite $CaMg_{2.3}Fe_{0.1}Al_{3.2}Si_{1.4}O_{10}(OH)_2$ (04-019-1584)
	Mullite $Al_{4.64}Si_{1.36}O_{9.68}$ (01-079-1453)
	Maghemite Fe_2O_3 (04-008-3650)

MGF-modified TSRC cured in water had higher peak intensities of analcime, katoite and grossular than the non-modified composite. Some quartz (shoulder at 2Θ: 26.2-26.3) and iron-containing calcium-silicate phase srebrodolskite (shoulders, e.g. 2Θ:31.98) formed in these samples after the first day of curing at 300°C (Table 3). A peak at 26.4 (found only in the pattern of glass-modified samples) is likely from keatite SiO_2 (04-007-1438). The samples with MGF were richer in silica already after the first curing day. The pattern shows a clear peak at 2Θ: 37.18, which likely belongs to sodium-aluminum silicate (04-015-8059). The peak strongly declines after 30 days.

Comparison of 15- and 30-day cured modified TSRC clearly demonstrates that MGF stabilize analcime. Analcime peaks at 2Θ: 15.921/30.64 are present only in the patterns of modified TSRC. Because of the analcime stabilization there is less cancrinite (peaks at 2Θ: 14.16, 19.2, 24.53, 32.86, 43.11) obtained through analcime→ cancrinite transition. There are higher intensity

peaks of iron-containing grossular (andradite, at 2Θ: 29.86, 33.4, 35.19, 36.79, 41.11), iron-magnesium silicate, khesinite and iron oxide peak at 2Θ: 30.1. Among the three reaction products, iron-containing grossular, iron-magnesium silicate and analcime, formed in samples of modified TSRC, the first two products enhanced the strength recovery and analcime participated in cracks' sealing.

Some mica-type mineral with the peaks at 2Θ: 20.22-20.26 was the same as for the samples without MGF. The mica minerals that fit the pattern included: paraganite-2M1 (01-083-2128); celadonite/muscovite 3T (04-021-4959); margarite 2M1 (04-013-3004) or potassium-aluminum-magnesium-iron silicate oxide hydroxide (01-079-6488(6487)). Similarly, some peaks could be ascribed to feldspars with decreased calcium (albite, calcian) or alkali feldspars (albite, orthoclase, sanidine). Additionally, presence of magnesium-containing mineral, polymorph of serpentine, lizardite, was possible in MGF-modified samples. Small amounts of magnesium could be coming from the reacting glass fibers. Magnesium minerals, in this case lizardite and khesinite, increase the strength of the cement matrix. High-temperature calcium silicate wollastonite formed only in glass-modified samples likely from silicon and calcium released by decomposing MGF.

As with the TSRC samples, silica dominated the XRD patterns of surface samples of TSRC-modified with MGF. Other possible phases included cancrinite, sodium-aluminum silicate, aegirine and feldspars with reduced calcium as in the case of the reference TSRC samples (Table 4). Based on the XRD test results, Figure 8 depicts a schematic of possible crystalline phase transitions in the matrix of TSRC samples cured at 300°C for different periods.

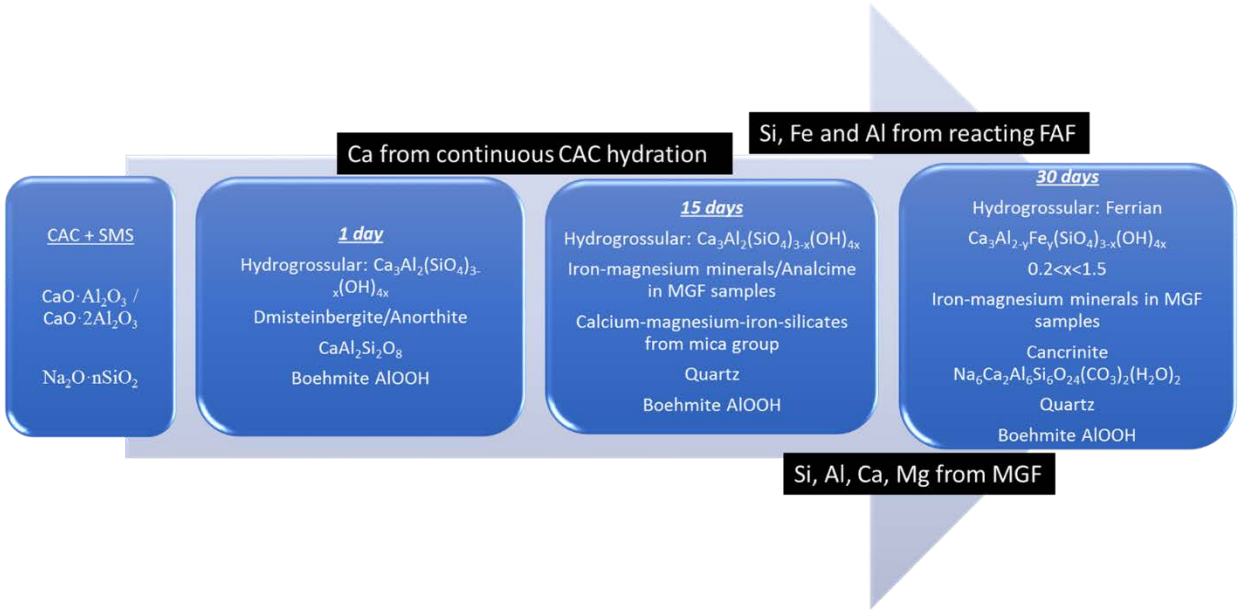

Figure 8. Crystalline phases formation and transitions with time for TSRC samples cured in water environment at 300°C.

Table 2. Major, minor and possible crystalline phases formed at the <u>surface</u> at 300°C after 15- or 30-day exposure of unmodified TSRC.

Major phases (ICDD numbers)	Minor phases (ICDD numbers)
1-day curing	
Analcime, $Na_{0.9}((Al_{0.9}Si_2)O_6)(H_2O)$ (01-076-6569) Grossular hydroxylian $Ca_3Al_2(SiO_4)_2(OH)_4$ (and other stoichiometries) (00-042-0570) Katoites $Ca_{2.916}Al_2Si_{1.092}O_{12}H_{7.632}$/ $Ca_3Al_2(SiO_4)_{1.53}(OH)_{5.88}$ (01-075-4213/04-014-984) Dmisteinbergite $CaAl_2Si_2O_8$ (04-011-5220) Corundum Al_2O_3 (01-073-1512)	Boehmite AlOOH (04-012-5050) Mullite $Al_{2.25}Si_{0.75}O_{4.875}$ (04-014-8459)
15-day curing	
Cancrinite $Na_{7.28}Ca_{0.64}(Si_6Al_6O_{24})(CO_3)_{1.65}(H_2O)_2$ / $Na_{7.28}Ca_{0.64}(Si_6Al_6O_{24})(CO_3)_{1.66}(H_2O)_2$ (01-081-9895/9893) Khesinite $CaMgFe_{2.2}Al_{1.7}Si_{1.1}O_{10}$ (04-013-3515) Quartz SiO_2 (01-070-8054) Some mica mineral	Sodium-aluminum-silicate $Na_8(Al(SiO_4)_6(OH)_2$ (00-040-0100) Maghemite-C Fe_2O_3 (00-039-1346) Analcime $Na_{7.2}Al_{7.2}Si_{16.8}O_{48}(H_2O)_8$ (04-013-2038) Andradite aluminian $Ca_3(Fe_{1.42}Al_{0.56})(SiO_4)_3$ (01-082-8676) Mullite $Al_{2.19}Si_{0.81}O_{4.901}$ (04-008-9530) Aegirine $NaFeSi_2O_6$ (04-015-8149) Paragonite $NaAl_3Si_3O_{10}(OH)_2$ (04-017-0660) Albite, calcian/albite $Na_{0.6}Ca_{0.4}Al_{1.4}Si_{2.6}O_8$/ $NaAlSi_3O_8$ (04-007-9876/01-080-3256)
30-day curing	
Silica SiO_2 (00-033-1161/04-008-7653) Aegirine aluminian $NaFe_{0.65}Al_{0.35}Si_2O_6$ (04-014-4678) Cancrinite $Na_{7.28}Ca_{0.64}(Si_6Al_6O_{24})(CO_3)_{1.65}(H_2O)_2$ (01-081-9895) Some mica mineral	Sodium aluminum silicate hydrate $0.99Na_2O \cdot Al_2O_3 \cdot 4.07\ SiO_2 \cdot 5.7H_2O$ (00-038-0328) Stishovite SiO_2 (04-007-3487) *Possible*: Microcline $K(AlSi_3O_8)$ (01-071-0955) Khesinite $CaMgFe_{2.2}Al_{1.7}Si_{1.1}O_{10}$ (04-013-3515) Mullite $Al_{4.868}Si_{1.132}O_{9.566}$ (01-079-1452) Sillimanite $Al_2O_3 \cdot SiO_2$ (00-001-0626) Amicite $K_2Na_2Si_4Al_4O_{16}(H_2O)_5$ (04-011-3051) Albite, calcian/albite $Na_{0.6}Ca_{0.4}Al_{1.4}Si_{2.6}O_8$/ $NaAlSi_3O_8$ (04-007-9876/01-080-3256)
<u>30-day plus 5-day healing</u>, major: Quartz/silica SiO_2 (00-033-1161/04-008-7653) Aegirine aluminian $NaFe_{0.65}Al_{0.35}Si_2O_6$ (04-014-4678) Carbonated sodium calcium aluminum silicate (Cancrinite) $Na_{7.28}Ca_{0.64}(Si_6Al_6O_{24})(CO_3)_{1.65}(H_2O)_2$ (01-081-9895) Some mica mineral	**<u>30-day plus 5-day healing</u>**, minor: Maghemite-C Fe_2O_3 (00-039-1346) *Possible*: Sanidine $K(Si_3Al)O_8$ (00-025-0618) Analcime $Na_{14.4}Al_{14.4}Si_{33.6}O_{96}(H_2O)_{16}$ (04-013-2040) Bohmite AlOOH (04-014-2197) Khesinite $CaMgFe_{2.2}Al_{1.7}Si_{1.1}O_{10}$ (04-013-3515) Mullite $Al_{4.868}Si_{1.132}O_{9.566}$ (01-079-1452) Amicite $K_2Na_2Si_4Al_4O_{16}(H_2O)_5$ (04-011-3051) Albite, calcian/albite $Na_{0.6}Ca_{0.4}Al_{1.4}Si_{2.6}O_8$/ $NaAlSi_3O_8$ (04-007-9876/01-080-3256)

Table 3. Major, minor and possible crystalline phases formed in matrix at 300°C after 1-,15- or 30-day exposure of MGF-modified TSRC.

Major phases (ICDD numbers)	Minor phases (ICDD numbers)
1-day curing	
Analcime $Na_{1.71}((Al_{1.806}Si_{4.194})O_{12}(H_2O)_{2.16}$ (01-075-8690) Dmisteinbergite $CaAl_2Si_2O_8$ (04-011-5220) Katoites $Ca_{2.916}Al_2Si_{1.092})_{12}H_{7.632}/Ca_3Al_2(SiO_4)_{1.53}(OH)_{5.88}$ (01-075-4213/04-014-9841) Quartz SiO_2 (01-089-8946) Grossular hydroxylian $Ca_3Al_2(SiO_4)_2(OH)_4$ (00-042-0570) Sodium-aluminum-silicate $NaAlSi_2O_6$ (04-015-8059) Corundum Al_2O_3 (04-008-3293) Sillimanite Al_2SiO_5 (00-022-0018)	Boehmite AlOOH (04-012-5050) Mullite $Al_{2.34}Si_{0.66}O_{4.83}$ (01-076-2579) Srebrodolskite $Ca_2Fe_2O_5$ (04-007-2756)
15-day curing	
Cancrinite $Na_{7.28}Ca_{0.64}(Si_6Al_6O_{24})(CO_3)_{1.65}(H_2O)_2/(Na_{7.05}Ca_{0.87})(Al_6Si_6O_{24})(CO_3)_{1.76}(H_2O)_2$ (01-081-9895/01080-6875) Analcime $Na_{0.9}((Al_{0.9}Si_2)O_6)(H_2O)$ (01-076-6569) Corundum Al_2O_3 (01-073-1512) Anorthite $CaAl_2Si_2O_8$ (04-012-1276) Khesinite $CaMgFe_{2.2}Al_{1.7}Si_{1.1}O_{10}$ (04-013-3515) Some mica mineral	Boehmite AlOOH (01-074-2895) SiO_2 (01-099-8948/01-077-8634) Fe_2SiO_4 (01-071-1400) Maghemite $Fe_{21}O_{31}(OH)$ (04-009-9615) Grossular, ferrian hydroxylian $Ca_3Al_{1.096}Fe_{0.904}(Si_{2.823}O_{11.292})(OH)_{0.708}$ /Grossular hydroxylian $Ca_3Al_2(SiO_4)_2(OH)_4$ (01-072-8446/00-042-0570)
30-day curing	
Cancrinite $Na_6Ca_{1.5}Al_6Si_6O_{24}(CO_3)_{1.6}$ (00-034-0176) Grossulars $Ca_3Al_{1.096}Fe_{0.904}(Si_{2.823}O_{11.292})(OH)_{0.708}$ /$Ca_3Al_2(SiO_4)_2(OH)_4$ /$Ca_{2.81}Al_{1.89}((SiO_4)_{2.38}(O_4H_4)_{0.62})$ (01-072-8446/00-031-0250/01-083-7410) Corundum Al_2O_3 (01-073-1512)	Bohmite AlOOH (04-010-5683) Tohdite $Al_5O_{7.5}(H_2O)_{0.5}$ (04-014-1755) Silica SiO_2 (00-011-0252) Maghemite-C Fe_2O_3 (00-039-1346) Andradite aluminium $Ca_{2.82}Fe_{1.20}Al_{0.98}(SiO_4)_3$ (04-020-1960) *Possible phases*: Albite $Na(AlSi_3O_8)$ (01-071-1150) Khesinite $CaMgFe_{2.2}Al_{1.7}Si_{1.1}O_{10}$ (04-013-3515) Sillimanite Al_2O_3 SiO_2 (00-001-0626) Wollastonite $CaSiO_3$ (00-042-0550) Lizardite $(Mg,Fe)_3Si_2O_5(OH)_4$ (00-050-1606)

Table 4. Major, minor and possible crystalline phases formed at surface under hydrothermal conditions at 300°C after 15- or 30 days exposure of MGF-modified TSRC.

Major phases (ICDD numbers)	Minor phases (ICDD numbers)
15 day curing	
Cancrinite $Na_{7.28}Ca_{0.64}(Si_6Al_6O_{24})(CO_3)_{1.65}(H_2O)_2$/ $Na_{7.28}Ca_{0.64}(Si_6Al_6O_{24})(CO_3)_{1.66}(H_2O)_2$ (01-081-9895/9893)	Sodium-aluminum-silicate $Na_8(Al(SiO_4)_6(OH)_2$ (00-040-0100)
	Analcime $Na_{7.2}Al_{7.2}Si_{16.8}O_{48}(H_2O)_8$ (04-013-2038)
Khesinite $CaMgFe_{2.2}Al_{1.7}Si_{1.1}O_{10}$ (04-013-3515)	Andradite aluminian $Ca_3(Fe_{1.42}Al_{0.56})(SiO_4)_3$ (01-082-8676)
Quartz SiO_2 (01-070-8054)	
	Mullite $Al_{2.19}Si_{0.81}O_{4.901}$ (04-008-9530)
	Aegirine $NaFeSi_2O_6$ (04-015-8149)
	Paragonite $NaAl_3Si_3O_{10}(OH)_2$ (04-017-0660)
	Reyerite $KCa_{14}Si_{24}O_{60}(OH)_5(H_2O)_5$ (00-017-0760)
30 day curing	
Quartz SiO_2 (04-015-7194)	*Possible*:
Cancrinite $Na_6Ca_{1.5}Al_6Si_6O_{24}(CO_3)_{1.6}$ (00-034-0176)	Albite, calcian $(Na, Ca)(SiAl)_4O_8$ (00-009-0456)
	Anorthoclase $NaAlSi_3O_8$ (04-006-8967)
Sodium aluminum silicate $Na_2Al_2Si_2O_8$ H_2O (00-010-0460)	Sanidine $K(AlSi_3O_8)$ (01-080-2108)
	Khesinite $CaMgFe_{2.2}Al_{1.7}Si_{1.1}O_{10}$ (04-013-3515)
Aegirine $NaFeSi_2O_6$ (04-014-4678)	Amicite $K_2Na_2Si_4Al_4O_{16}(H_2O)_5$ (04-011-3051)

The first forming phases, crystallizing shortly after the cement set in TSRC, are generally hydration- and SMS-reaction products of CAC. They include hydrogrossular, feldspars (dmisteinbergite and anorthite) and boehmite. At longer exposure times, garnets (various stoichiometries of hydrogrossular) become dominant. Continuous slow reactions of FAF introduce additional aluminum, silicon, iron and magnesium into the crystalline phases. Garnets with higher silicon content and with aluminum partially substituted by ferric iron replace earlier formed grossular; boehmite and silica contents noticeable increase. Additionally, mica group calcium-magnesium and calcium-magnesium-iron silicates form in the matrix. The slow reactions of FAF contributing such crystals-building ions as aluminum, silicon, iron and magnesium result in the recoveries of compressive strength for damaged samples. MGF become an additional source of silica, aluminum, calcium, and some magnesium and iron. These ions stabilize analcime for longer time, preventing its conversion into cancrinite and improving cracks sealing. Additional silica from MGF crystalizes in the fractures further filling them. MGF decomposition in alkali cement environments also introduces ions that form magnesium and iron-containing phases increasing strength of the matrix. MGF reacts slowly, and its sealing effect becomes more noticeable after longer curing times in samples exposed to 300°C for 15 or 30 days. Since XRD analyses could not unambiguously identify many of the smaller peaks especially for the surface samples, to compliment XRD phase identification Raman analyses of cracks areas were conducted on samples exposed to steam conditions after the imposed compressive damage and healing periods.

3.5 Raman analyses of crack areas for long-term cured MGF-modified and unmodified TSRC samples

Figure 9 shows a Raman spectrum of a crack area for a 15-day cured TSRC sample. The pattern unambiguously represents crystalline silica, a major phase filling the cracks after 15 and 30 days

of curing for both control and modified samples. In addition to silica, Raman showed spectra corresponding to iron-containing mineral aegirine in the spectra after longer curing times when fly ash reactions proceed to release iron (Figure 10). This correlates with the XRD results.

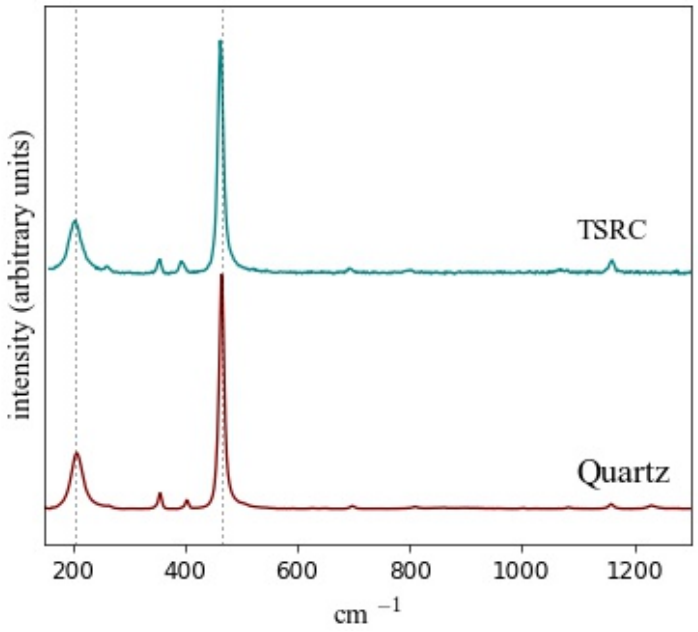

Figure 9. Raman spectrum of MGF-modified TSRC sample after 15 days of curing at 300°C in water environment and patterns of quartz matching the spectrum.

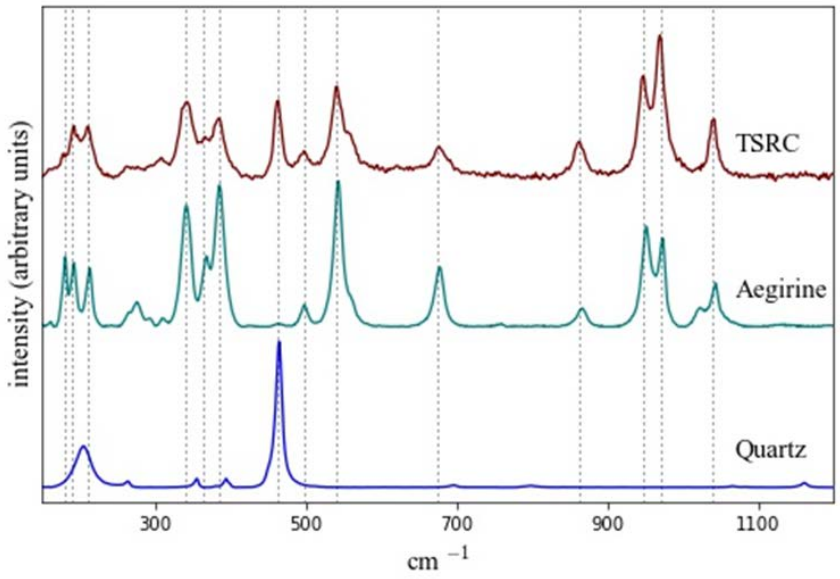

Figure 10. Raman spectrum of MGF-modified TSRC sample after 15 days of curing at 300°C in water environment and patterns of quartz and aegirine corresponding to the spectrum.

Another two phases are unmistakably present in the spectra of the filled-crack areas including bohmite and analcime (Figure 11). Both could be found in the samples even after short curing time of the first 5 days of cracks healing.

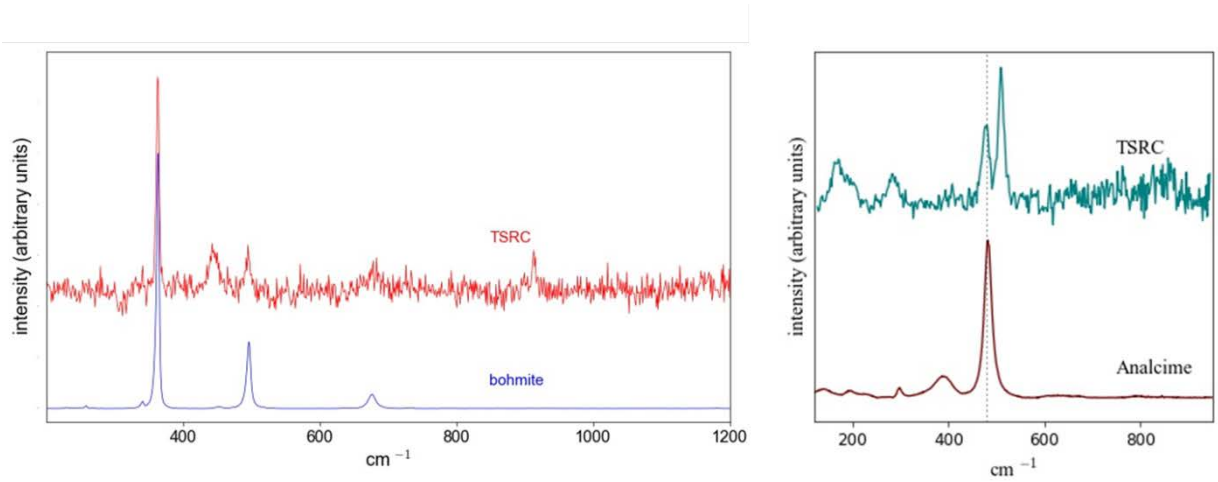

Figure 11. Raman spectra of TSRC-MCF sample after 15 days of curing at 300°C in water environment and patterns of bohmite and analcime matching the spectra.

After longer curing time of 30 days spectrum matching that of albite was found in TSRC samples modified with glass fibers (Figure 12).

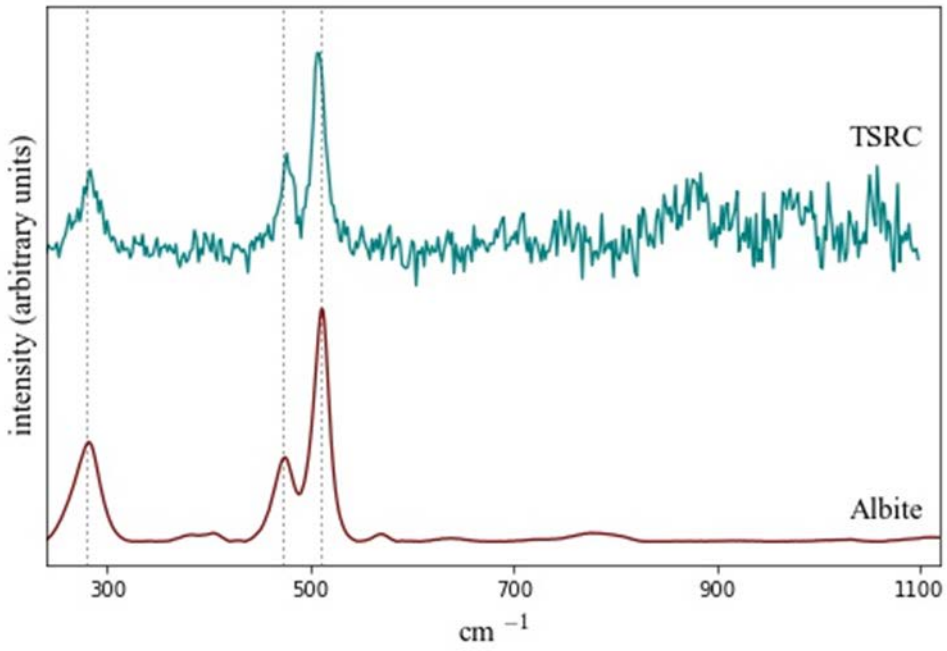

Figure 12. Raman spectrum of TSRC-MGF sample after 30 days of curing at 300°C in water environment and pattern of albite matching the spectrum.

However, for the most part, silica spectrum dominated the spectra of the crack areas or complex overlapping spectra of many phases were obtained for the samples (Figure 13). Relatively broad peaks with shoulders indicated multiple phases contributing to the signal. In addition to earlier mentioned silica, bohmite, albite and high-temperature zeolite (amicite, in this case), the spectrum could be formed by feldspar minerals with varying calcium and potassium contents. The presence of feldspars is likely since albite matched a spectrum at another location and XRD patterns suggested possibility of these minerals in TSRC samples. Changes in calcium content after long curing times may be explained by increased contribution of silicon, aluminum and alkali metals from fly ash and glass fibers participating in high-temperature reactions.

Raman results confirmed XRD findings on surface composition of crack sealing phases in TSRC samples that for the most part included silica, high-temperature zeolites (analcime and amicite), sodium-iron-silicate (aegirine), aluminum oxide hydroxide (bohmite) and feldspar minerals with varied calcium and alkali metals contents.

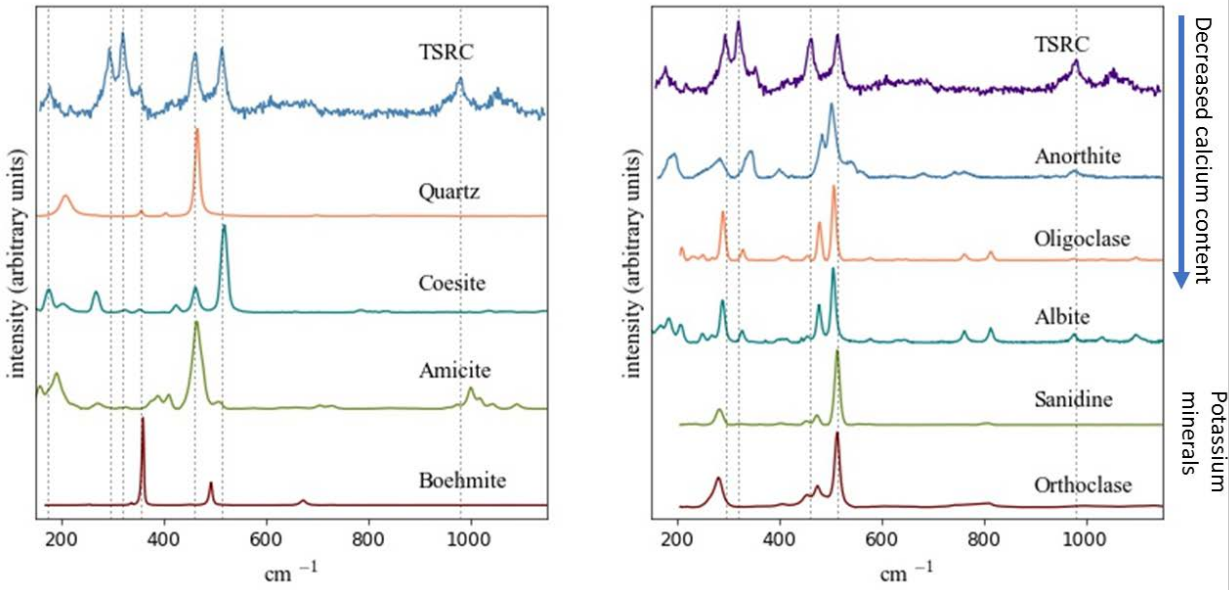

Figure 13. Raman spectrum of TSRC-MGF sample after 30 days of curing at 300°C in water environment and reference patterns matching the spectrum.

Based on the information obtained by XRD and Raman tests, Figure 14 proposes phase transitions occurring at the surface and in the fractures of TSRC samples as the curing progresses. The major crystalline phases participating in cracks' sealing from early curing times are zeolite analcime and silica mostly from sodium silicate and calcium aluminate cement early reactions. As the curing continues analcime converts to cancrinite through carbonation, so the content of analcime declines. Sodalite forms, and more silica precipitates because of alkali dissolution of fly ash and MGF (for MGF-modified samples) with release of silicon and aluminum ions. Silica remains the main sealing phase throughout the healing, and especially after longer curing times when FAF and MGF dissolution releases more of silicon ions. Alkali dissolution of FAF and MGF also contributes more aluminum, some iron and alkalis to the pool of reacting ions after longer curing. They form (sodium, potassium, calcium)-aluminum-silicates

from feldspar group of minerals with varied calcium and alkali metal contents replacing originally formed calcium-aluminum silicate feldspars, anorthite and dmisteinbergite. Sodium iron silicate, aegirine, also precipitates in the cracks.

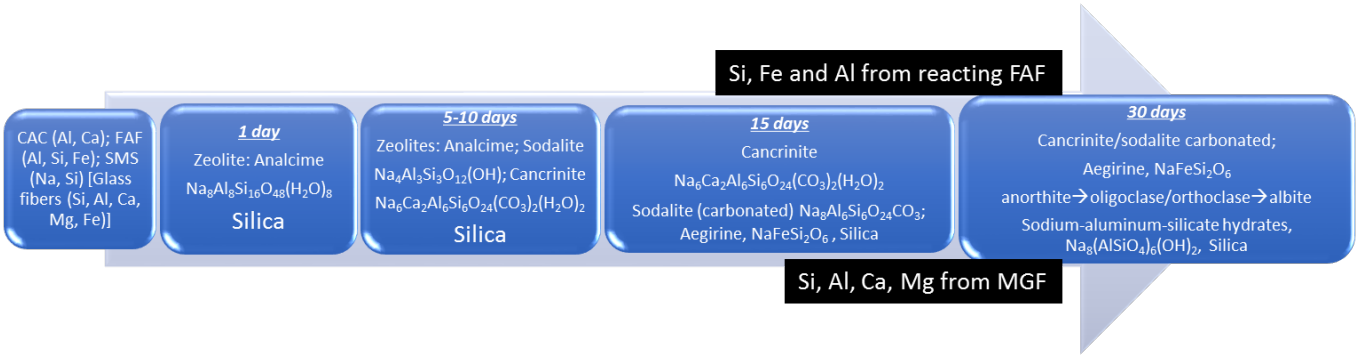

Figure 14. Crystalline phases formation and transitions with time at the surface and in the cracks of TSRC samples cured in water environment at 300°C.

4. Discussion

The healing capacity of TSRC continued after the 30 days of hydrothermal curing at 300°C. The composite sustained a moderate increase in YM remaining moderately brittle in nature. Its compressive strength increased to 2410 psi after 30 days from 1740 psi after 1 day. Similarly, OPC/SiO_2 remained moderately brittle with compressive strength of 2965 psi. A conspicuous increase of YM was observed from MGF-modified TSRC composite as a function of autoclaving time; YM value increased by nearly 3-fold to 409 x 10^3 psi at 300°C- 30-day autoclave curing in plain water, compared with that of 1-day curing, thereby resulting in mechanical transition from moderate brittle nature to brittle one due to alkali dissolution and reaction of MGF, followed by densification of cement. The compressive strength of TSRC/MGF composite increased to 2860 psi after 30 days from 1840 psi at 1 day.

Although a grate recovery of 117% was observed for MGF-modified TSRC after a day initial curing, the extended autoclaving time to 30 days resulted in the reduction of recovery rate to 61%. Unlike modified TSRC, unmodified TSRC after the same 30-day curing exhibited 86% recovery of compressive strength. The low recovery of only 36% was observed for unmodified OPC/SiO_2 after 30 days of curing.

The sealing became more efficient for the MGF-modified samples made by a 30-day long curing. In fact, the wider cracks representing a brittle fracture mode were sealed after only a 5-day healing, instead of 10-day treatment which was required for 1-day cured samples. The most likely explanation for this reduced healing time was the presence of reactive ionic species as healing promoters and accelerators released by the slow continuous disintegration of MGF under alkaline environment of the composite at 300°C after long-term curing. These ionic reactants released from MGF interacted with counter reactants in the composite to form and precipitate new sealing and plugging solid state phases in crack spacing. Hence, even after longer initial curing, the samples still possessed the sealing capacity in the presence of MGF, thereby confirming MGF's role as a healing aid. Consequently, such a slow disintegration of MGF

healing aid was a very important factor for a long-term healing. Additionally, the increase in MGF's disintegration along with prolonged curing time likely created amorphous phases which could help in developing smaller cracks that fill faster because of ductile nature of amorphous phase. In fact, the widths of cracks at 30-day curing ages were relatively smaller than that were imposed by the damage of a 1-day aged samples; for instance, an average cracks size was ~0.15-0.35 mm after 30-day curing vs. 0.2-0.5 mm after the first day. This is one of the reasons why the cracks in aged composites were readily sealed.

The XRD studies and Raman surface analyses showed that the early-forming phases in TSRC composites, crystallizing shortly after the cement set at 300^{o}C-1-day age, are for the most part hydration and SMS-reaction products of CAC. They include hydrogrossular, feldspars (dmisteinbergite and anorthite) and boehmite. At longer curing times, garnets (various stoichiometries of hydrogrossular) become predominant. Continuous slow reactions of FAF introduce additional aluminum, silicon, iron and magnesium into the crystalline phases. Garnets with higher silicon content and with aluminum partially substituted by ferric iron replace earlier formed grossular; boehmite and silica contents noticeably increase. Additionally, mica group calcium-magnesium and calcium-magnesium-iron silicates form in the matrix. The slow reactions of FAF contributing such crystals-building ions as aluminum, silicon, iron and magnesium result in the recoveries of compressive strength for damaged samples. MGF become an additional source of silica, aluminum, calcium, and some magnesium and iron. These ions stabilize analcime for longer time, preventing its conversion into cancrinite and improving cracks sealing. Additional silica from MGF crystalizes in the fractures further filling them. MGF decomposition in alkali cement environments also introduces ions that form magnesium and iron-containing phases increasing strength of the matrix. Aluminum and silicon crystallization reactions are relatively slow so that sealing effect of MGF that involves aluminum- and silicon-containing phases becomes more noticeable after longer curing times in samples exposed to 300^{o}C for 15 or 30 days. On the other hand, magnesium and iron form stable crystalline phases faster, so that contribution of MGF to the strength recovery happens at earlier curing ages. Relating this information to a lower recovery rate of compressive strength at 30-day initial curing than that of unmodified composite at same curing age, such a lack of strength recovery may be due to the formation of these new iron-related reaction products, but independent of excellent crack sealing efficacy.

Regarding the crack sealing, most cracks included silica, high-temperature zeolites (analcime and amicite), sodium-iron-silicate (aegirine), aluminum oxide hydroxide (bohmite) and feldspar minerals with varied calcium and alkali metals contents. The major crystalline phases participating in crack sealing from early curing times are zeolite analcime and silica mostly from sodium silicate and calcium aluminate cement early reactions. As the curing continues analcime converts to cancrinite through carbonation, so the content of analcime declines. Another zeolite, sodalite, forms and more silica precipitates because of alkali dissolution of FAF and MGF (for MGF-modified samples) with release of silicon and aluminum ions. Silica remains the main sealing phase throughout the healing, and especially after longer curing times when FAF and MGF dissolution releases more silicon ions. In addition to silicon, alkali dissolution of FAF and MGF contributes more aluminum, some iron and alkalis to the pool of reacting ions after longer curing. They form (sodium, potassium, calcium)-aluminum-silicates from feldspar group of minerals with varied calcium and alkali metal contents replacing originally formed calcium-

aluminum silicate feldspars, anorthite and dmisteinbergite. Sodium iron silicate, aegirine, also precipitates in the cracks.

5. Conclusions

TSRC, shown to have outstanding self-healing properties after short initial curing times, keeps its healing capacity after 30 days of hydrothermal curing at 300^{o}C before the damage, recovering 86% of its compressive strength after a 5-day healing period. For comparison, OPC-based formulation recovered only 36% of its strength under the same conditions. The strength recovery was not as good for TSRC modified with MGF (61%). This was likely due to the increased brittleness of the MGF-modified composite that resulted in hard-to-heal cracks when damaged after longer curing times.

The crack-sealing ability of TSRC improved after the curing time before the damage was increased from 1 to 15 and then to 30 days. The sealing happened faster for MGF-modified TSRC than for non-modified one.

The phases responsible for TSRC healing formed due to the continuous slow reactions of FAF that contributed such crystals-building ions as aluminum, silicon, iron and magnesium to the formation of new phases. Presence of MGF improved sealing stabilizing the main sealing phases, zeolite analcime and silica.

The main crystalline contributors to cracks sealing and strength recoveries of MGF-modified and non-modified TSRC composites differed.

Acknowledgement

This publication was based on the work supported by the Geothermal Technologies Office in the US Department of Energy (DOE) Office of Energy Efficiency and Renewable Energy (EERE), under the auspices of the US DOE, Washington, DC, under contract No. DE-AC02-98CH 10886. Raman data were acquired in SoMAS' Nano-Raman Molecular Imaging Laboratory (NARMIL), a community facility dedicated to environmental sciences' applications and founded with NSF-MRI grant OCE-1336724.

REFERENCES

Ahn, T.-H., & Kishi, T. (2010). Crack self-healing behavior of cementitious composites incorporating various mineral admixtures. *Journal of Advanced Concrete Technology, 8*, 171–186.

Amin, M. N., Kim, J.-S., Lee, Y., & Kim, J.-K. (2009). Simulation of the thermal stress in mass concrete using a thermal stress measuring device. *Cement and Concrete Research, 39*, 154–164.

Edvardsen, C. (1999). Water permeability and autogenous healing of cracks in concrete. *American Concrete Institute Materials Journal, 96*, 448–454.

Gill, S. K., Pyatina, T., & Sugama, T. (2012). Thermal shock-resistant cement. In *Transactions - Geothermal Resources Council* (Vol. 36 1).

Huang, H., Ye, G., & Damidot, D. (2013). Characterization and quantification of self-healing behaviors of microcracks due to further hydration in cement paste. *Cement and Concrete Research*, *52*, 71–81.

Huang, H., Ye, G., & Damidot, D. (2014). Effect of blast furnace slag on self-healing of microcracks in cementitious materials. *Cement and Concrete Research*, *60*, 68–82.

Li, V. C., & Yang, E. H. (2007). Self-Healing in Concrete Materials in Self Healing Materials: An Alternative Approach to 20 Centuries of Materials Science. In R. Hull, R. M. J. Osgood, J. Parisi, & H. Warlimont (Eds.), *Springer Series in materials science* (pp. 161–193).

McCulloch, J., Gastineau, J., Bour, D., & Ravi, K. (2003). No Title. In *Geothermal Resources Council Transactions* (pp. 12–15). Geothermal Resources Council.

Pyatina, T., & Sugama, T. (2014a). Set controlling additive for thermal-shock-resistant cement. In *Transactions - Geothermal Resources Council* (Vol. 38).

Pyatina, T., & Sugama, T. (2014b). Toughness improvement of geothermal well cement at up to 300^{o}C: Using carbon microfiber. *Journal of Composite Materials*, *4*, 177–190.

Pyatina, T., & Sugama, T. (2015). Use of carbon microfibers for reinforcement of calcium aluminate-class F fly ash cement activated with sodium meta-silicate at up to 300°C. In *Transactions - Geothermal Resources Council* (Vol. 39).

Pyatina, T., Sugama, T., & Ronne, A. (2016). Self-repairing geothermal well cement composites. In *Transactions - Geothermal Resources Council* (Vol. 40).

Qian, S. ., Zhou, J. ., & Schlangen, E. (2010). Influence of curing condition and pre-cracking time on the self-healing behavior of engineered cementitious composites. *Cement & Concrete Composite*, *32*, 686–693.

Ravi, K., Bosma, M., & Gastebled, O. (2002). Improve the Economics of Oil and Gas Wells by Reducing the Risk of Cement Failure. In *IADC/SPE Drilling Conference*. Dallas: Society of Petroleum Engineers. https://doi.org/https://doi.org/10.2118/74497-MS

Reinhardt, H.-W., & Jooss, M. (2003). Permeability and self-healing of cracked concrete as a function of temperature and crack width. *Cement & Concrete Research*, *33*, 981–985.

Sahmaran, M. G., Yildirim, G., & Erdem, T. K. (2013). Self-healing capability of cementitious composites incorporating different supplementary cementitious materials. *Cement & Concrete Composites*, *35*, 89–101.

Sahmaran, M., Keskin, S. B., Ozerken, G., & Yaman, I. O. (2008). Self-healing of mechanically-loaded self consolidating concrete. *Cement & Concrete Composite*, *30*, 872–879.

Sisomphon, K., Copuroglu, O., & Koenders, E. A. B. (2012). Self-healing of surface cracks in mortars with expansive additive and crystalline additive. *Cement & Concrete Research*, *34*, 566–574.

Sui, L., Luo, M., Yu, K., Xing, F., Li, P., Zhou, Y., & Chen, C. (2018). Effect of engineered cementitious composite on the bond behavior between fiber-reinforced polymer and

concrete. *Composite Structures*, *184*(January), 775–788. https://doi.org/10.1016/j.compstruct.2017.10.050

Teodoriu, C., Kosinowski, C., Amani, M., Schubert, J., & Shadravan, A. (2013). Wellbore integrity and cement failure at HPHT conditions. *International Journal of Engineering and Applied Sciences*, *2*, 1–13.

Termkhajornkit, P., Nawa, T., & Yamashiro, Y. (2009). Self-healing ability of fly ash-cement systems. *Cement & Concrete Composites*, *31*(195–203).

Yang, Y., Michael, D. L., Yang, E., & Li, V. C. (2009). Autogenous Healing of Engineered Cementitious Composites under Wet-Dry Cycles. *Cement and Concrete Research*, *39*, 382–390.

Yang, Z., Hollar, J., He, X., & Shi, X. (2011). A self-healing cementitious composite using oil core/silica gel shell microcapsules. *Cement & Concrete Composites*, *33*, 506–512.

Zhijun, T., Yanjun, Z., & Jianghong, J. (2013). Technology for improving life of thermal recovery well casing. *Advances in Petroleum Exploration and Development*, *5*, 71–76.